Organic & Biomolecular Chemistry

PAPER

View Article Online
View Journal | View Issue

Cite this: *Org. Biomol. Chem.*, 2018, **16**, 5474

A theoretical study on NHC-catalysed enantioselective cycloaddition of ketenes and 3-aroylcoumarins: mechanism and enantioselectivity†

Ramón J. Zaragozá, *[a] María J. Aurell *[a] and Miguel A. González-Cardenete [b]

Received 3rd May 2018,
Accepted 11th July 2018

DOI: 10.1039/c8ob01035h

rsc.li/obc

NHC-catalysed enantioselective cycloaddition of ketenes to 3-aroylcoumarins to yield dihydrocoumarin-fused dihydropyranones has been investigated using DFT methods at the B3LYP/6-31G* and MPWB1K/6-311G** computational levels. Two plausible mechanisms have been studied: the "ketene-first" mechanism A and the "coumarin-first" mechanism B. An analysis of the activation Gibbs free energies involved in the two competitive pathways makes it possible to rule out the pathway associated with the "coumarin-first" mechanism B. The first step of the "ketene-first" mechanism A is the formation of zwitterionic intermediate **IN1-*Z*** *via* a nucleophilic attack of NHC **1** on ketene **2**. A [4 + 2] cycloaddition through the nucleophilic attack of enolate **IN1-*Z*** on the conjugated double bond of the benzoyl group of coumarin **3**, *via* **TS3-*SS*-a2** or **TS3-*RR*-a2**, yields **IN3**. Finally, the extrusion of the catalyst through **TS5** leads to the final products, either **4-*SS*** or **4-*RR***. Enantioselectivity observed in the experimental results is determined in the transition states **TS3-*SS*-a2**/**TS3-*RR*-a2**. In this pathway, the intramolecular hydrogen-bonding between the hydroxyl group of the **IN1-*Z*** adduct and the carbonyl oxygen of the original ketene group directs the final stereochemistry throughout the entire process.

1. Introduction

In recent years, N-heterocyclic carbenes (NHCs) have been successfully utilised as catalysts in organocatalytic reactions.[1,2] Catalysis in organic chemistry not only makes an acceleration of the reactions possible or improves selectivity but also enables the generation of intermediates distinct from the inherent chemistry of the reagents. The use of NHCs has introduced a new set of elementary steps that take place *via* discrete reactive species, including acyl anion **I** and homoenolate **II** equivalents, and acyl azolium **III**/**IV** (see Scheme 1). Nearly all NHC-catalysed reactions proceed at room temperature without the need for stringent exclusion of air and do not generate reaction by-products. Variation of the catalyst, the base, or reaction conditions can profoundly influence the reaction outcomes. The use of chiral NHCs has allowed the development of catalysed asymmetric reactions, having made significant progress possible over the past decade.[3] Interestingly, while acyl anion **I** and homoenolate **II** equivalents are nucleophilic species, allowing the inversion of the normal reactivity of the aldehyde precursors, *umpolung* reactivity, acyl azolium cations **III** and **IV** are activated electrophilic species with a unique and unprecedented chemistry.[1–4]

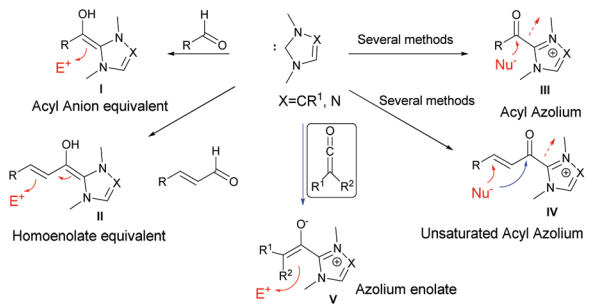

Scheme 1 Intermediates generated by the reaction of NHCs.

The addition of NHCs to ketenes provides an approach to form azolium enolates **V** (see Scheme 1) that is an alternative to the methods involving rearrangements of acyl anion equivalents. Azolium enolates, generated *in situ* by the nucleophilic addition of a NHC to an aryl(alkyl)-disubstituted ketene, were employed as dienophiles in [4 + 2] annulations with enones[1,5]

[a]*Departamento de Química Orgánica, Universidad de Valencia, Dr. Moliner 50, 46100 Burjassot, Valencia, Spain. E-mail: Ramon.J.Zaragoza@uv.es*
[b]*Instituto de Tecnología Química (UPV-CSIC), Universitat Politècnica de Valencia-Consejo Superior de Investigaciones Científicas, Avda. de los Naranjos s/n, 46022 Valencia, Spain*

†Electronic supplementary information (ESI) available. See DOI: 10.1039/c8ob01035h

or benzoyldiazenes,[1,6] in [2 + 2] cycloadditions with *N*-protected imines,[1,7,8] α-keto aldehydes,[1] diazenedicarboxylates,[9] benzaldehydes[10] or *N*-sulfinylanilines,[1] in [3 + 2] cycloadditions with oxaziridines,[1] in [2 + 2 + 2] cycloadditions with isocyanates[1,11] and in esterification of ketenes.[1,12]

In these types of reactions, it is suggested that the NHC initially reacts with ketene to yield the azolium enolate **V**. Then, enolate **V** reacts with the appropriate species to yield the final product (see for example, mechanism A in Scheme 2).[4–14] However, Ye and co-workers[7] suggest two possible mechanisms for the carbene-catalysed Staudinger reaction of ketenes with imines (Scheme 2). As for denoted "ketene-first" mechanism A, the nucleophilic catalyst initially attacks the ketene to generate a NHC–ketene zwitterionic intermediate, which is followed by the reaction between this enolate and the imine to form a second intermediate. Finally, the cyclization of this intermediate to the final β-lactam and the expulsion of the NHC close the reaction pathway. However, in the "imine-first" mechanism B, the nucleophilic catalyst initially attacks the imine to generate a NHC–imine zwitterionic intermediate. This intermediate attacks the ketene and after the expulsion of NHC gives the final β-lactam.

Liu and co-workers[15] performed a DFT study on the two proposed reaction mechanisms and concluded that the "ketene-first" mechanism A is much more feasible than the "imine-first" mechanism B in the NHC-catalysed Staudinger reaction. Subsequently, Tang and co-workers[16] carried out a theoretical investigation toward the [4 + 2] cycloaddition of ketenes with *N*-benzoyldiazenes catalysed by NHC and came to the conclusion that in this case, the "diazene-first" mechanism (similar to the "imine-first" mechanism B) is more favorable than the "ketene-first" mechanism A. Recently, these same authors[17] conducted a theoretical study toward the [4 + 2] cycloaddition of ketenes with 1-azadienes catalysed by NHC. The results revealed that the "ketene-first" mechanism is more energetically favorable than the "azadiene-first" one (similar to the "imine-first" mechanism B).

Recently, Ye and co-workers[18] reported a catalysed [4 + 2] cycloaddition (using different NHCs, for example **1**) of ketenes **2** and 3-aroylcoumarins **3** to give the corresponding dihydrocoumarin-fused multi-substituted dihydropyranones **4** in high yields with high enantioselectivity (Scheme 3). Solvent screening revealed that the reaction performed better in toluene than in DCM or THF in terms of enantioselectivity (42–98% ee). This reaction is very convenient and attractive; however, there are still some questions that need to be solved: (a) what is the possible mechanism?: "ketene-first" mechanism A or "coumarin-first" mechanism B. (b) What is the possible detailed mechanism? (c) Is it possible to predict the final stereochemistry?

Our interest in organocatalysis, more specifically in the participation of NHCs as catalysts,[19] prompted us to perform some density functional theory (DFT) studies on the molecular mechanisms of these interesting reactions. Herein, a DFT study for the NHC-catalysed (NHC = **1**, Ar═Ph) reaction of ketene **2** (R═Me) with 3-aroylcoumarin **3** (Ar═Ph) yielding dihydrocoumarin-fused dihydropyranones **4** is presented. As a result, two possible mechanisms have been studied: "coumarin-first" or mechanism B and "ketene-first" or mechanism A, and within each one, different options have been studied. The "coumarin-first" mechanism is totally new and has not been studied to date. Two possible channels have been studied: channel B1 and B2. With regard to the second mechanistic alternative, for the "ketene-first" mechanism (mechanism A), only the initial step has been studied in similar systems, but the course of such a mechanism (subsequent reaction with coumarin) has been studied for the first time. Three different mechanistic options, channel A1, channel A2 and channel A3, have been studied. We believe that our results are important for understanding this kind of organocatalytic reaction, and thus providing valuable insights into the rational design of similar reactions with high enantioselectivity.

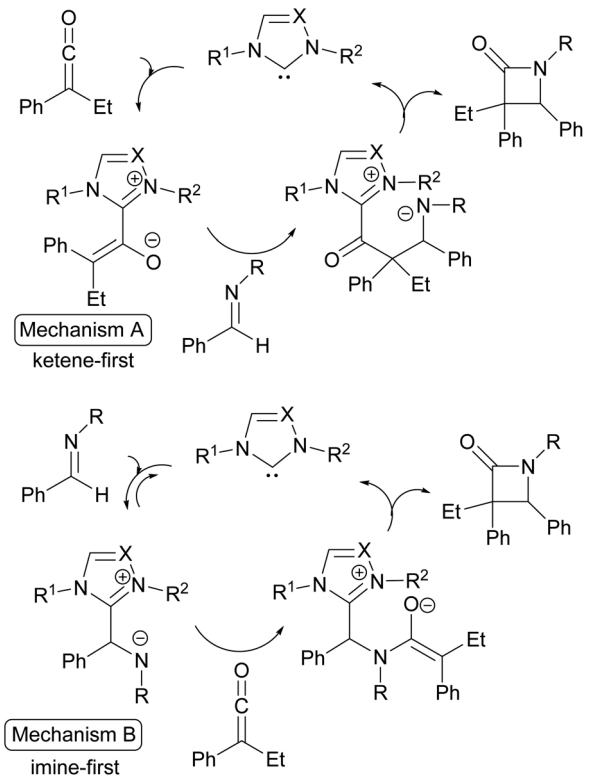

Scheme 2 Two possible catalytic mechanisms in the carbene-catalysed Staudinger reaction.

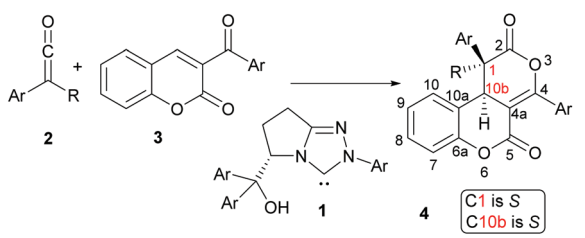

Scheme 3 Cycloaddition of ketenes **2** and 3-aroylcoumarins **3**.

2. Results and discussion

As a computational model, we have selected NHC **1** (Ar═Ph), ketene **2** (R═Me) and 3-aroylcoumarin **3** (Ar═Ph) because they construct the simplest reactant structures and also afford relatively high yields and enantiomeric excess values. As shown in Scheme 3, it should be noted that there are two chiral centers (1 and 10b) in the final product **4**, and also there are some intermediates with stereocenters or *E*/*Z* double bonds (see Schemes 4 and 5), so we use letters to represent the chirality (*R*/*S*) or the stereochemistry (*E*/*Z*).

The global mechanistic possibilities are reflected in Scheme 4: "ketene-first" mechanism A and the "coumarin-first" mechanism B. In mechanism A, two clearly differentiated routes have been studied. In the first one, the conversion of intermediate **IN1** to intermediate **IN3** takes place in a single stage through **TS2**. This is the mechanism suggested by Ye and co-workers.[18] In the second route, this conversion takes place through several stages (**TS3** and **TS4**).

Firstly, in order to determine which of the two mechanistic possibilities is more reasonable, we will only consider the channels that lead to the major enantiomer of **4** (**4-*SS***; C1 and C10b with *S* configuration). Later, we will study and compare the routes that lead to both enantiomers (**4-*SS*** and **4-*RR***).

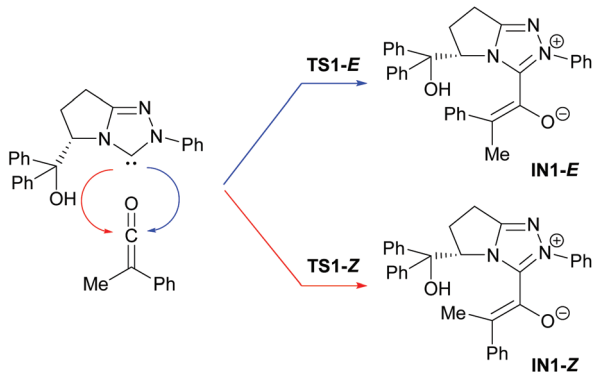

Scheme 5 Formation of zwitterionic intermediates **IN1-*E*/IN1-*Z***.

The free energy profiles are shown in Fig. 1 (see also Tables S1–S6 and Fig. S1–S23 of the ESI† for more details of the energies and geometries of the species involved).

2.1. Computational methods

All calculations were carried out with the Gaussian 09 suite of programs.[20] Initially, due to the large size of the molecules, DFT[21] calculations were carried out using the B3LYP[22]

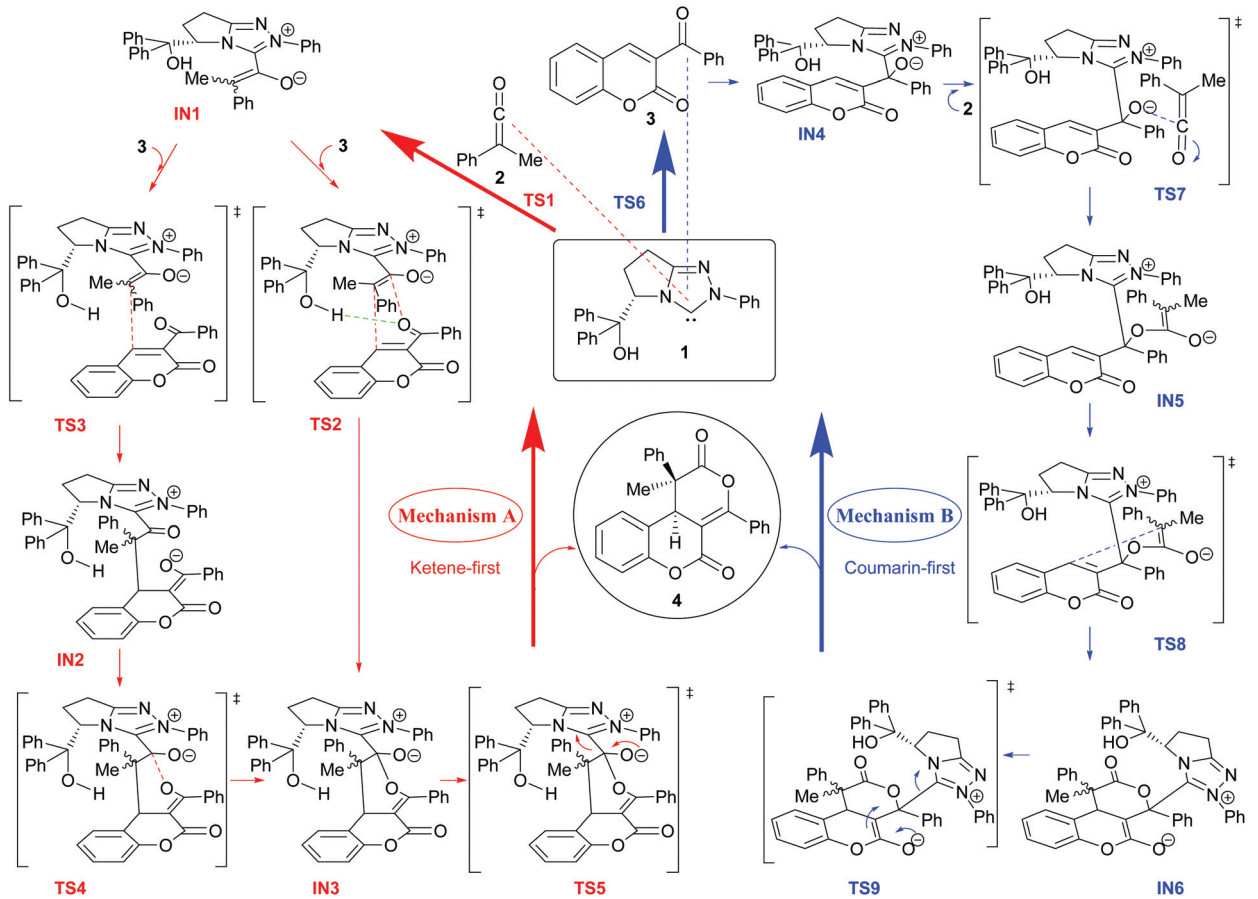

Scheme 4 Two proposed reaction channels: the "ketene-first" mechanism A (left in red) and the "coumarin-first" mechanism B (right in blue).

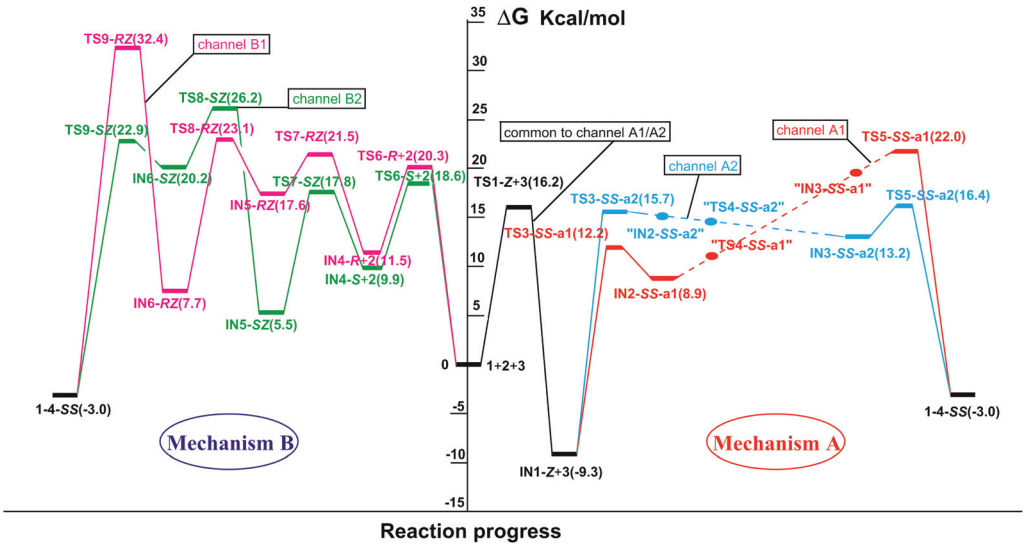

Fig. 1 Free energy profiles, at the B3LYP/6-31G* level in the gas phase, of mechanism A (right) and mechanism B (left). Mechanism A: channel A1 (in red) and channel A2 (in blue). Mechanism B: channel B1 (in pink) and channel B2 (in green). The dashed line indicates a hypothetical way of the reaction. The hypothetical species of the reaction are indicated by quotation marks.

exchange–correlation functionals, together with the standard 6-31G* basis set, in the gas phase.[23] For each of the transition states (TS), a careful search was carried out to locate the most stable conformers. To this end, the distances, angles and dihedrals involved in the TS were maintained. The parts of the molecule susceptible to conformational changes were altered manually. Each of the conformers was optimized. Only the most stable conformers are presented.

The stationary points were characterized by frequency computations in order to verify that transition states have one and only one imaginary frequency. The intrinsic reaction coordinate (IRC) pathways[24] were traced in order to check the energy profiles connecting each TS to the two associated minima of the proposed mechanisms using the second order González–Schlegel integration method (see Fig. S1–S16 of the ESI†).[25] In the case of problematic IRCs (flat PES in the vicinity of the TS), a relaxed scan was performed. The values of enthalpies, entropies and free energies were calculated with the standard statistical thermodynamics at 298.15 K and 1 atm.[23]

Once the most favorable channels for mechanism A and mechanism B were determined, single-point calculations at the MPWB1K/6-311G** level in toluene were made for the species involved in these channels. Finally, for the most plausible mechanism, the species involved in this mechanism were totally optimized in toluene, using the MPWB1K hybrid meta functional[26] together with the 6-311G** basis set.[23] This level of theory has shown good results for combinations of thermochemistry and thermochemical kinetics in processes including weak interactions.[26] Solvent effects of toluene were taken into account by full optimization using the polarisable continuum model (PCM) as developed by Tomasi's group[27] in the framework of the self-consistent reaction field (SCRF).[28]

2.2. Mechanism A

The first step of the reaction is the formation of zwitterionic intermediates **IN1-*E*/IN1-*Z*** *via* the nucleophilic attack of NHC **1** on both sides of ketene **2** *via* the transition states **TS1-*E*/TS1-*Z*** (Scheme 5). The Gibbs free energy barriers *via* **TS1-*E*/TS1-*Z*** are 19.8 and 17.4 kcal mol^{-1}, respectively (Tables S1 and S2 of the ESI†), indicating that the *Z* face attack is energetically more favorable than the *E* face attack in dynamics. Also, the following TSs of this pathway have a smaller energy and therefore, it is reasonable to exclude the reaction pathway through an *E* intermediate in the following parts.

Ye and co-workers[18] proposed a model for stereochemical outcome: "the enolate generated by the addition of the NHC to ketene favors *Z*-isomer which minimizes the steric repulsion. The hydrogen-bonding between the hydroxy group of the NHC-ketene adduct and aroyl group of the coumarin derivative directs the facial selectivity. The *endo* transition state of the Diels–Alder reaction is favoured and results in the *cis*-cycloadduct observed". The transition state of the Diels–Alder reaction corresponds to **TS2** represented in Scheme 4. However, all attempts to locate **TS2** gave disappointing results. Nevertheless, it was possible to locate other possible reaction pathways that are represented in Fig. 1: channel A1, channel A2 and channel A3 (see Fig. S17 of the ESI†).

2.2.1. Channel A1. In this pathway, the intermolecular hydrogen-bonding between the hydroxyl group of the **IN1-*Z*** adduct and the carbonyl oxygen of the benzoyl group of coumarin **3** directs the final stereochemistry throughout the entire process (see Scheme 6 and Fig. S18, S19 of the ESI†). As shown in Scheme 6 and Fig. 1, the step-by-step [4 + 2] cycloaddition proceeds through two elementary steps: initially, the nucleophilic attack of enolate **IN1-*Z*** on the conjugated double bond

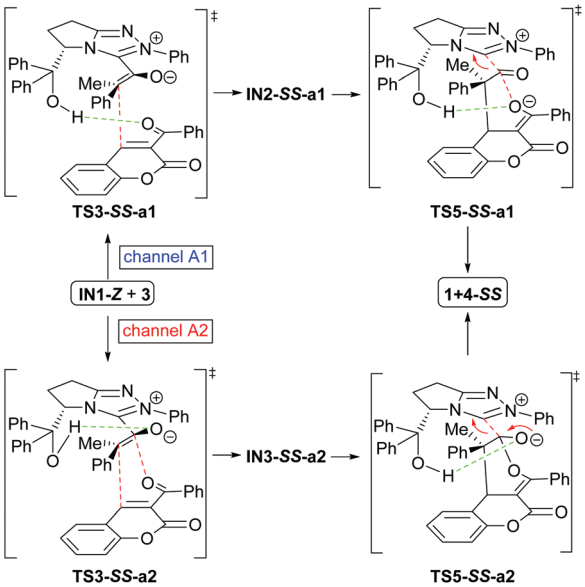

Scheme 6 Formation of final product **4-*SS*** from **IN1-*Z*** and **3**. Channels A1 (up) and A2 (down). Hydrogen bonds are shown in green. Bonds that are forming or breaking are shown in red.

of the benzoyl group of coumarin **3** (**TS3-*SS*-a1**) to give **IN2-*SS*-a1**, and finally the ring closure and simultaneous dissociation of the catalyst through **TS5-*SS*-a1** to release the final product **4-*SS***. It should be noted that **IN2-*SS*-a1** evolves to the final product without going through **TS4-*SS*-a1** and **IN3-*SS*-a1** (Scheme 6 and Fig. 1). This can be seen in the corresponding IRCs (see Fig. S4 of the ESI†). While the IRC of **TS3-*SS*-a1** connects the starting products **IN1-*Z*** + **3** with the intermediate **IN2-*SS*-a1** (see Fig. S3 of the ESI†), the IRC of **TS5-*SS*-a1** connects the intermediate **IN2-*SS*-a1** with the final products **1** + **4-*SS*** (see Fig. S4 of the ESI†). The IRC of **TS5-*SS*-a1** also shows that part of the energy increase is due to the initial approach of O3 to carbonyl C2. In fact, in that TS, the bond O3–C2 is almost formed, while the extrusion of the NHC has barely begun (see Fig. S4 of the ESI†).

The Gibbs free energy barriers *via* **TS3-*SS*-a1** and **TS5-*SS*-a1** from **1** + **2** + **3** are 12.2 and 22.0 kcal mol^{-1}, respectively (Table S2 of the ESI†), indicating that the **TS5-*SS*-a1** is the rate-determining step of channel A1.

2.2.2. Channel A2. In this pathway, the hydrogen bond that directs the final stereochemistry throughout the entire process corresponds to the intramolecular hydrogen-bonding between the hydroxyl group of the **IN1-*Z*** adduct and the carbonyl oxygen of the original ketene group (see Scheme 6 and Fig. S18, S19 of the ESI†). This route may seem *a priori* more unfavorable since it does not facilitate the approximation of coumarin **3** to intermediate **IN1-*Z***. However, as we will see later, it turns out to be less energetic than channel A1.

As shown in Scheme 6 and Fig. 1, the [4 + 2] cycloaddition proceeds through a two-stage one-step mechanism. The nucleophilic attack of enolate **IN1-*Z*** on the conjugated double bond of the benzoyl group of coumarin **3** (**TS3-*SS*-a2**) gives directly **IN3-*SS*-a2** without going through **IN2-*SS*-a2** and **TS4-*SS*-a2**. In intermediate **IN3-*SS*-a2**, both bonds C1–C10b and O3–C2 are already formed. The corresponding IRC shows a totally asynchronous process; the bond O3–C2 does not start to form until the bond C1–C10b is almost formed (see Fig. S5 of the ESI†). In this case, the hydrogen-bonding between the hydroxyl group of the **IN1-*Z*** adduct and the carbonyl oxygen of the original ketene group increases the nucleophilicity of this carbonyl. At the same time, the absence of the hydrogen bond between the hydroxyl group of the **IN1-*Z*** adduct and O3 increases the nucleophilic character of the latter (compare **TS3-*SS*-a1** and **TS3-*SS*-a2** in Fig. S19 of the ESI†). This facilitates the attack of O3 on carbonyl C2. Finally, the extrusion of the catalyst through **TS5-*SS*-a2** leads to the final product **4-*SS***.

The Gibbs free energy barriers *via* **TS3-*SS*-a2** and **TS5-*SS*-a2** from **1** + **2** + **3** are 15.7 and 16.4 kcal mol^{-1}, respectively (Table S2 of the ESI†). Both TSs have fairly similar energies, with the free energy of **TS5-*SS*-a2** being slightly higher. This route is more favorable than route A1 in about 5.6 kcal mol^{-1}.

It should be noted that another channel connecting intermediate **IN2-*SS*-a1** to intermediate **IN3-*SS*-a2** was found (see channel A3, Table S2, Fig. S17/S22 and Scheme S1 of the ESI†). This variant does not improve the most favorable channel A2 from the energy point of view.

2.3. Mechanism B

As shown in Scheme 4 and Fig. 1, mechanism B follows the assumption that it should be coumarin **3** that combines with the NHC catalyst in advance. There are four steps involved in mechanism B, including the nucleophilic attack of NHC **1** on coumarin **3**, then the two stepwise bonding processes of the O3 atom with the C2 atom and the C1 atom with the C10b atom, and finally the release of the product and the catalyst.

The first step of the reaction is the formation of zwitterionic intermediates **IN4-*R*/IN4-*S*** *via* the nucleophilic attack of NHC **1** on the *Re* or *Si* face of coumarin **3** *via* the transition states **TS6-*R*/TS6-*S*** (Scheme 7). Both possibilities have been considered giving rise to channels B1 (*Si* attack) and B2 (*Re* attack). In both cases, the intermolecular hydrogen-bonding between the hydroxyl group of NHC **1** and the carbonyl oxygen of the benzoyl group of coumarin **3** facilitates the attack of the NHC (see Scheme 8 and Fig. S20, S21 of the ESI†).

2.3.1. Channel B1. After the initial attack of NHC **1** on the *Si* face of coumarin **3** through **TS6-*R*** (ΔG = 20.3 kcal mol^{-1} from 1 + 2 + 3) to give the intermediate **IN4-*R***, the next two steps are the stepwise [4 + 2] cycloaddition reactions. The first

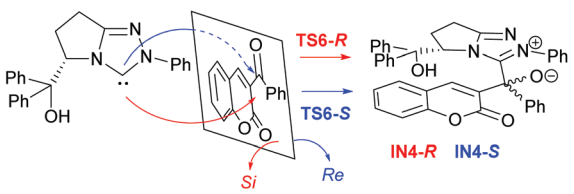

Scheme 7 Formation of zwitterionic intermediates **IN4-*R*/IN4-*S***.

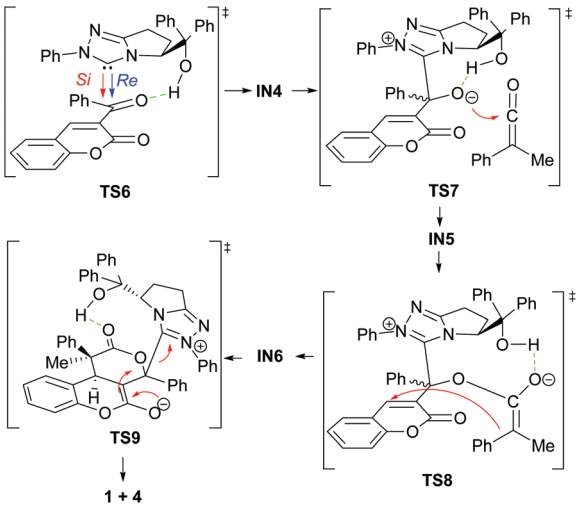

Scheme 8 Mechanism B.

process of cycloaddition is initiated by the *endo* attack of zwitterion **IN4-*R*** on ketene **2** through **TS7-*RZ*** (ΔG = 21.5 kcal mol^{-1} from **1** + **2** + **3**) to give **IN5-*RZ*** (see Scheme 8). The most unfavorable *exo* attack, which would lead to the intermediate **IN5-*RE*** with the *E*-double bond, is excluded in the following stages. In **TS7-*RZ***, the hydrogen bond between the hydroxyl group of NHC **1** and the O3 of **3** is still maintained.

The second process of cycloaddition through **TS8-*RZ*** (ΔG = 23.1 kcal mol^{-1} from **1** + **2** + **3**) involves the bonding reaction between the C1 atom and the C10b atom. In this stage, the stereochemistry of both carbons present in the final product is determined. In this case, the hydrogen bond between the hydroxyl group of **1** and the carbonyl oxygen of ketene **2** is more favorable. Finally, catalyst **1** through **TS9-*RZ*** (ΔG = 32.4 kcal mol^{-1} from **1** + **2** + **3**) is released. This last step is the rate-determining step of channel B1.

2.3.2. Channel B2. Channel B2 proceeds in a similar manner to channel B1, but passing through **TS6-*S***, **TS7-*SZ***, **TS8-*SZ*** and **TS9-*SZ***. The **TS8-*SZ*** (ΔG = 26.2 kcal mol^{-1} from **1** + **2** + **3**) corresponds to the rate-determining step of this channel. This route is more favorable than route B1 by about 6.2 kcal mol^{-1} (compare **TS9-*RZ*** and **TS8-*SZ***).

Taking both mechanisms discussed above (mechanism A and mechanism B) into consideration, the energy barrier of mechanism A (channel A2) is 16.4 kcal mol^{-1} for the rate-determining step *via* **TS5-*SS*-a2** while it is 26.2 kcal mol^{-1} for mechanism B (channel B2) *via* **TS8-*SZ***.

2.4. MPWB1K/6-311G** in toluene//B3LYP/6-31G* in the gas-phase for channel A2 and channel B2

In order to ensure that the conclusions drawn at the B3LYP/6-31G* level are valid at different levels of calculations, single-point calculations at the MPWB1K/6-311G** level in toluene were made of the species involved in channel A2 and channel B2.

The free energy profiles are shown in Fig. 2 (see also Table S4 of the ESI† for more details on the energies).

There are notable changes in the energies of the species. An increase in stability is especially pronounced in **TS3-*SS*-a2**/**TS5-*SS*-a2** (channel A2) and **TS8-*SZ***/**TS9-*SZ*** (channel B2). As a result of these changes, **TS1-*Z*** (ΔG = 19.4 kcal mol^{-1} from **1** + **2** + **3**) becomes the rate-determining step of channel A2 and **TS6-*S*** (ΔG = 22.9 kcal mol^{-1} from **1** + **2** + **3**) becomes the rate-determining step of channel B2. We can conclude that mechanism A (channel A2) is more energetically favorable.

Therefore, it should be noted that **TS8-*SZ*** determines the stereochemistry of the final products (**4-*SS***) through mechanism B (channel B2). The **TS8-enant** (see Table S4 and Fig. S21 of the ESI†) was also calculated. This would give rise to **4-*RR*** which is the enantiomeric form obtained experimentally in a smaller proportion. The result is that its energy (ΔG = 8.2 kcal mol^{-1} from **1** + **2** + **3**) is lower than that obtained for

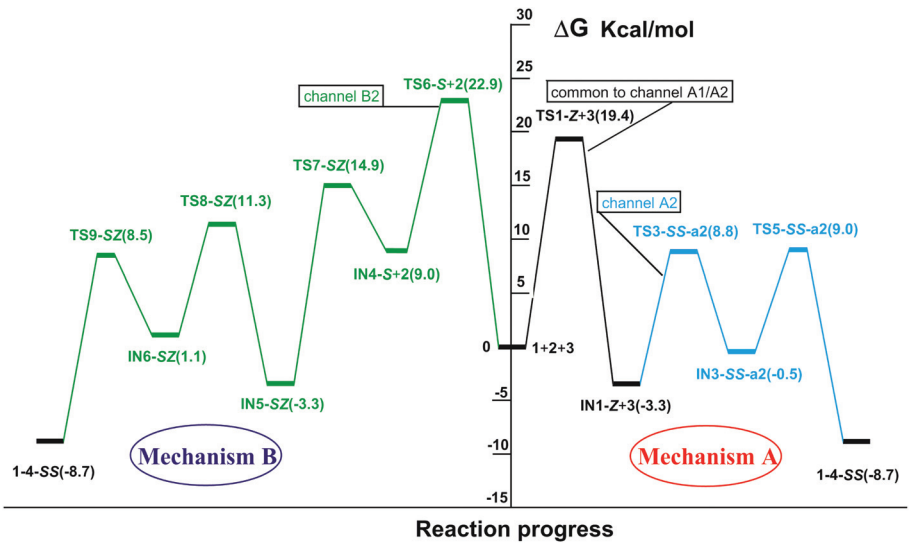

Fig. 2 Free energy profiles, at MPWB1K/6-311G**, in toluene//B3LYP/6-31G*, in the gas phase, of channel A2 (in blue) and channel B2 (in green).

TS8-*SZ* (ΔG = 11.3 kcal mol^{-1} from **1** + **2** + **3**) and would lead to a greater proportion of the final product **4-*RR*** *versus* **4-*SS***. This result does not fit the experimental result and is an additional circumstance to rule out mechanism B *versus* mechanism A.

In this way, the first two questions are resolved: (a) what is the possible mechanism?: "ketene-first" mechanism A and (b) what is the possible detailed mechanism?: mechanism A (channel A2).

The third question would remain: (c) is it possible to predict the final stereochemistry?

2.5. Prediction of enantioselectivity

In order to determine the enantiomeric excess observed experimentally, we carried out a detailed theoretical study at a high level and with a solvent effect. The selected mechanism corresponds to the most favorable channel A2 from the energy point of view. We studied the two routes that lead to both enantiomers: mechanism A2-*SS* (corresponding to mechanism A2 previously studied) and mechanism A2-*RR* (variation of the A2 mechanism leading to the 4-*RR* enantiomer). Species involved in this mechanism were optimized in toluene, using the MPWB1K/6-311G** level. This level of theory has shown good results for combinations of thermochemistry and thermochemical kinetics in processes including weak interactions. The relative energies (ΔG) associated with the conversion of **1** + **2** + **3** to **4-*SS*** and **4-*RR*** are given in Fig. 3 (see also Tables S5 and S6 of the ESI†). The geometries are shown in Fig. S23 of the ESI.†

The inclusion of the solvent and the MPWB1K/6-311G** level does not produce significant geometric changes in the species involved in mechanism A2-*SS* (compare **TS1-*Z***, **TS3-*SS*-a2** and **TS5-*SS*-a2** in Fig. S18 and S19† with the same TSs in Fig. S23 of the ESI†). However, there are notable changes in the energies of the species. An increase in stability of all the species with respect to **1** + **2** + **3** is observed. This increase in stability is especially pronounced in **TS3-*SS*-a2**, **IN3-*SS*-a2**, **TS5-*SS*-a2** and **1–4-*SS***. While **TS1-*Z***, **TS3-*SS*-a2** and **TS5-*SS*-a2** at the B3LYP/6-31G* level have similar energies (ΔG = 16.2, 15.7 and 16.4 kcal mol^{-1}, respectively. See Fig. 1), these same transition states at the MPWB1K/6-311G** level have different energies (ΔG = 15.4, −3.6 and −5.7 kcal mol^{-1}, respectively. See Fig. 3).

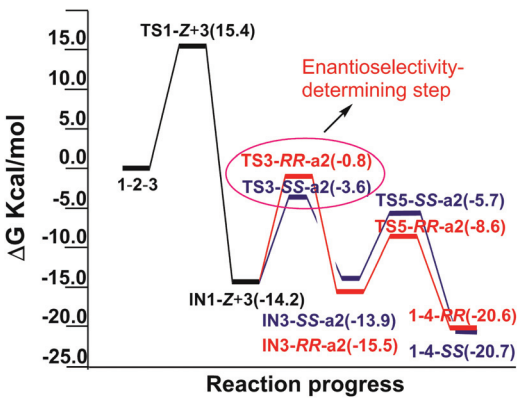

Fig. 3 Free energy profiles (ΔG) of mechanism A2 at the MPWB1K/6-311G** level, in toluene. Mechanism A2-*SS* isomer (in blue) and mechanism A2-*RR* isomer (in red).

The reaction pathway that starts from **IN1-*Z*** and leads to the enantiomer **4-*RR*** (mechanism A2-*RR* in Fig. 3) is similar to that found for the enantiomer **4-*SS*** (mechanism A2-*SS* in Fig. 3). The transition states **TS3-*RR*-a2** and **TS5-*RR*-a2** have relative energies (ΔG) of −0.8 and −8.6 kcal mol^{-1}, respectively (see Fig. 3). These relative energies are similar to the relative energies of transition states **TS3-*SS*-a2** and **TS5-*SS*-a2**. As seen in Fig. 3, the rate-determining step for the conversion of intermediate **IN1-*Z*** (common to both mechanisms) in the final products **4-*SS*** and **4-*RR*** corresponds to the transition states **TS3-*SS*-a2** and **TS3-*RR*-a2**, respectively. It should be noted that these transition states determine the stereochemistry of the final products and therefore correspond to the enantioselectivity-determining step. The transition state **TS3-*SS*-a2** is 2.8 kcal mol^{-1} which is more stable than the transition state **TS3-*RR*-a2**. These results are in agreement with the experimental outcome of 87% ee.[18]

What is the origin of stereoselectivity?

If we observe the structures of **TS3-*SS*-a2** and **TS3-*RR*-a2** (see Fig. S23 of the ESI†), there are two main causes that facilitate their stabilization: hydrogen-bonding and π–π-stacking. In both cases, there is an intramolecular hydrogen-bonding between the hydroxyl group of the **IN1-*Z*** adduct and the carbonyl oxygen of the original ketene group. This hydrogen-bonding does not seem to be the main cause of the energy difference between the two TSs. The distance H···O in **TS3-*SS*-a2** is 2.291 Å and 1.871 Å in **TS3-*RR*-a2**. The smaller distance in **TS3-*RR*-a2** apparently would favour the greater stabilization of **TS3-*RR*-a2** compared to **TS3-*SS*-a2**, which is not the case. Therefore, it must be the stabilization produced by π–π-stacking, the origin of the stereoselectivity.[2] Although both transition states show π–π-stacking between the aromatic ring of the chromenone moiety and the aromatic ring of the ketene fragment, there are differences. In **TS3-*SS*-a2**, the distance between both aromatic rings is 4.002 Å and the dihedral angle between the aromatic rings is 29.9° (ideally, it should be 0°). For **TS3-*RR*-a2**, these measurements are 4.140 Å and 31.5°. Thus, the stabilization due to π–π-stacking in **TS3-*SS*-a2** is superior to that of **TS3-*RR*-a2**.

In addition, in **TS3-*SS*-a2**, there is greater stabilization of the negative charge that is being generated in O3. An analysis of natural charges (see Fig. S23 of the ESI†) shows the presence of the following charges for **TS3-*SS*-a2**: −0.72 (O3), +0.49 (C2) and +0.49 (C between the two N of the triazole). Similarly, for **TS3-*RR*-a2**: −0.72 (O3), +0.49 (C2) and +0.46 (C between the two N of the triazole). The difference in charges is minimal, but in the case of **TS3-*SS*-a2**, the O3 is closer to the carbon between the two N of the triazole (2.771 Å against 3.008 Å for **TS3-*RR*-a2**). This produces an increase in stability due to favorable electrostatic interactions.

In view of these results, it is quite reasonable to think that the presence of substituents other than hydrogen on the aromatic ring of the chromenone moiety and the aromatic ring of

the ketene fragment can modify the π–π-stacking, and therefore the energy and the ratio between **TS3-*SS*** and **TS3-*RR***.

3. Summary and conclusions

A theoretical study of the NHC-catalysed enantioselective cycloaddition of ketenes and 3-aroylcoumarins to give the corresponding dihydrocoumarin-fused multi-substituted dihydropyranones has been carried out.

Initially, at the B3LYP/6-31G* level in the gas phase, two possible mechanisms were studied:

1. "Ketene-first" mechanism A. In this mechanism, the nucleophilic catalyst initially attacks the ketene to generate a NHC–ketene zwitterionic intermediate, which is followed by the reaction between this enolate and the aroylcoumarin; cyclization and expulsion of NHC close the reaction pathway.

2. "Coumarin-first" mechanism B. In this mechanism, the nucleophilic catalyst initially attacks the aroylcoumarin to generate an NHC–aroylcoumarin intermediate. This intermediate attacks the ketene and after the expulsion of NHC gives the final product.

In conclusion, mechanism A through channel A2 is more favorable. The first step of the reaction is the formation of zwitterionic intermediate **IN1-*Z*** *via* the nucleophilic attack of NHC **1** on ketene **2** *via* the transition state **TS1-*Z***. The second step is the [4 + 2] cycloaddition which takes place through a two-stage one-step mechanism. In this step, the nucleophilic attack of enolate **IN1-*Z*** on the conjugated double bond of the benzoyl group of coumarin **3**, through **TS3-*SS*-a2**, yields **IN3-*SS*-a2**. Finally, the extrusion of the catalyst through **TS5-*SS*-a2** leads to the final product **4-*SS***. In this pathway, the hydrogen bond that directs the final stereochemistry throughout the entire process corresponds to the intramolecular hydrogen-bonding between the hydroxyl group of the **IN1-*Z*** adduct and the carbonyl oxygen of the original ketene group.

The theoretical studies carried out at the MPWB1K/6-311G** level in toluene indicate that the observed enantioselectivity in the experimental results is determined in the transition states **TS3-*SS*-a2**/**TS3-*RR*-a2**.

The most probable cause of the origin of stereoselectivity is the π–π-stacking between the aromatic ring of the chromenone moiety and the aromatic ring of the ketene fragment in **TS3**. From the experimental point of view, the modification of the substituents in these aromatic rings can alter the ratio between the final stereoisomers.

Conflicts of interest

There are no conflicts to declare.

Acknowledgements

This study was supported by intramural grant 201680I008 from the Spanish Government (Consejo Superior de Investigaciones Científicas).

References

1 D. M. Flanigan, F. Romanov-Michailidis, N. A. White and T. Rovis, *Chem. Rev.*, 2015, **115**, 9307.
2 Y. Wang, D. Wei and W. Zhang, *ChemCatChem*, 2018, **10**, 338.
3 J. Mahatthananchai and J. W. Bode, *Acc. Chem. Res.*, 2014, **47**, 696.
4 X. Bugaut and F. Glorius, *Chem. Soc. Rev.*, 2012, **41**, 3511.
5 Y.-R. Zhang, H. Lv, D. Zhou and S. Ye, *Chem. – Eur. J.*, 2008, **14**, 8473.
6 X.-L. Huang, L. He, P.-L. Shao and S. Ye, *Angew. Chem., Int. Ed.*, 2009, **48**, 192.
7 Y.-R. Zhang, L. He, X. Wu, P.-L. Shao and S. Ye, *Org. Lett.*, 2008, **10**, 277.
8 N. Duguet, C. D. Campbell, A. M. Z. Slawin and A. D. Smith, *Org. Biomol. Chem.*, 2008, **6**, 1108.
9 D. Wei, Y. Zhu, C. Zhang, D. Sun, W. Zhang and M. Tang, *J. Mol. Catal. A: Chem.*, 2011, **334**, 108.
10 M. Zhang, D. Wei, Y. Wang, S. Li, J. Liu, Y. Zhu and M. Tang, *Org. Biomol. Chem.*, 2014, **12**, 6374.
11 X.-N. Wang, L.-T. Shen and S. Ye, *Org. Lett.*, 2011, **13**, 6382.
12 X.-N. Wang, H. Lv, X.-L. Huang and S. Ye, *Org. Biomol. Chem.*, 2009, **7**, 346.
13 X.-N. Wang, L.-T. Shen and S. Ye, *Chem. Commun.*, 2011, **47**, 8388.
14 J. Douglas, K. B. Ling, C. Concellón, G. Churchill, A. M. Z. Slawin and A. D. Smith, *Eur. J. Org. Chem.*, 2010, 5863.
15 K. Tang, J. Wang, X. Cheng, Q. Hou and Y. Liu, *Eur. J. Org. Chem.*, 2010, 6249.
16 W. Zhang, Y. Zhu, D. Wei, Y. Li and M. Tang, *J. Org. Chem.*, 2012, **77**, 10729.
17 Y. Ran, M. Tang, Y. Wang, Y. Wang, X. Zhang, Y. Zhu, D. Wei and W. Zhang, *Tetrahedron*, 2016, **72**, 5295.
18 T.-Y. Jian, X.-Y. Chen, L.-H. Sun and S. Ye, *Org. Biomol. Chem.*, 2013, **11**, 158.
19 (*a*) M. J. Aurell, L. R. Domingo, M. Arnó and R. J. Zaragozá, *Org. Biomol. Chem.*, 2016, **14**, 8338; (*b*) L. R. Domingo, R. J. Zaragozá and M. Arnó, *Org. Biomol. Chem.*, 2011, **9**, 6616; (*c*) L. R. Domingo, R. J. Zaragozá and M. Arnó, *Org. Biomol. Chem.*, 2010, **8**, 4884.
20 M. J. Frisch, *et al.*, *Gaussian 09, Revision A.02*, Gaussian, Inc., Wallingford, CT, 2009.
21 (*a*) R. G. Parr and W. Yang, *Density Functional Theory of Atoms and Molecules*, Oxford University Press, New York, 1989; (*b*) T. Ziegler, *Chem. Rev.*, 1991, **91**, 651.
22 (*a*) A. D. Becke, *J. Chem. Phys.*, 1993, **98**, 5648; (*b*) C. Lee, W. Yang and R. G. Parr, *Phys. Rev. B: Condens. Matter Mater. Phys.*, 1988, **37**, 785.
23 W. J. Hehre, L. Radom, P. von R. Schleyer and J. A. Pople, *Ab initio Molecular Orbital Theory*, Wiley, New York, 1986.
24 K. Fukui, *J. Phys. Chem.*, 1970, **74**, 4161.
25 (*a*) C. González and H. B. Schlegel, *J. Phys. Chem.*, 1990, **94**, 5523; (*b*) C. González and H. B. Schlegel, *J. Chem. Phys.*, 1991, **95**, 5853.

26 Y. Zhao and D. G. Truhlar, *J. Phys. Chem. A*, 2004, **108**, 6908.
27 (*a*) J. Tomasi and M. Persico, *Chem. Rev.*, 1994, **94**, 2027; (*b*) B. Y. Simkin and I. Sheikhet, *Quantum Chemical and Statistical Theory of Solutions-A Computational Approach*, Ellis Horwood, London, 1995.
28 (*a*) E. Cances, B. Mennunci and J. Tomasi, *J. Chem. Phys.*, 1997, **107**, 3032; (*b*) M. Cossi, V. Barone, R. Cammi and J. Tomasi, *Chem. Phys. Lett.*, 1996, **255**, 327; (*c*) V. Barone, M. Cossi and J. Tomasi, *J. Comput. Chem.*, 1998, **19**, 404.